Identifying the Critical Factors Governing Translaminar Pressure Differential Through a Compartmental Model

Omkar G. Kaskar,[1] David Fleischman,[2] Yueh Z. Lee,[2] Brian D. Thorp,[2] Andrey V. Kuznetsov,[1] and Landon Grace[1]

[1]North Carolina State University, Raleigh, North Carolina, United States
[2]University of North Carolina at Chapel Hill, Chapel Hill, North Carolina, United States

Correspondence: Landon Grace, North Carolina State University, Campus Box 7910, Raleigh, NC 27695, USA; lgrace2@ncsu.edu.

Submitted: December 3, 2018
Accepted: June 18, 2019

Citation: Kaskar OG, Fleischman D, Lee YZ, Thorp BD, Kuznetsov AV, Grace L. Identifying the critical factors governing translaminar pressure differential through a compartmental model. *Invest Ophthalmol Vis Sci*. 2019;60:3204–3214. https://doi.org/10.1167/iovs.18-26200

Purpose. The effective management of glaucoma is hindered by an incomplete understanding of its pathologic mechanism. While important, intraocular pressure (IOP) alone is inadequate in explaining glaucoma. Non-IOP–mediated risk factors such as cerebrospinal fluid (CSF) pressure have been reported to contribute to glaucomatous optic neuropathy. Due to the difficulty associated with experimental measurement of the salient variables, such as the retrobulbar CSF pressure, porosity of the subarachnoid space (SAS), and especially those concerned with the perioptic SAS, there remains a limited understanding of the CSF behavior contributing to the translaminar pressure gradient (TLPG), hypothesized to be a critical factor in the development of glaucoma.

Method. An integrated compartmental model describing the intracranial and orbital CSF dynamics, coupled with intraocular dynamics, is developed based on first principles of fluid mechanics. A sensitivity analysis is performed to identify anatomic characteristics that significantly affect the retrobulbar subarachnoid space (RSAS) pressure and, consequently, the TLPG.

Results. Of the 28 parameters considered, the RSAS pressure is most sensitive to CSF flow resistance in the optic nerve SAS and the potential lymphatic outflow from the optic nerve SAS into the orbital space. A parametric study demonstrates that a combination of resistance in the range of $1.600 \times 10^{12} - 1.930 \times 10^{12}$ Pa s/m^3 (200.0 − 241.3 mm Hg min/mL) with 5% to 10% lymphatic CSF outflow yields RSAS pressures that are consistent with the limited number of studies in the literature.

Conclusions. The results suggest that a small percentage of lymphatic CSF outflow through the optic nerve SAS is likely. In addition, flow resistance in the orbital CSF space, hypothesized to be a function of patient-specific optic nerve SAS architecture and optic canal geometry, is a critical parameter in regulating the RSAS pressure and TLPG.

Keywords: CSF dynamics, translaminar pressure gradient, glaucoma, numerical modeling, optic nerve SAS

It is estimated that about 5.9 million people will be bilaterally blind from primary open angle glaucoma (POAG) by 2020, making glaucoma second only to cataract among visual disorders.[1] The disease is often characterized by elevated intraocular pressure (IOP). However, a significant subset of POAG patients were reported to have a statistically normal IOP, a condition called normal tension glaucoma (NTG).[2–4] Although it is accepted that IOP reduction alters the progression of glaucoma, it has been reported in some cases that the disease continues to progress even after the IOP has been lowered. This indicates that factors other than an elevated IOP play a role in the progression of glaucoma. Based on the observations that the ICP is lower in patients suffering from NTG as compared to nonglaucomatous control subjects,[5,6] recent studies suggest that the difference between IOP and intracranial pressure (TLPG) may play a crucial role in understanding the progression of glaucoma.[7] The current work is predicated upon the hypothesis that the TLPG is not a simple function of IOP and intracranial or spinal (lumbar puncture) pressure, but is influenced by the CSF pressure immediately adjacent to the posterior sclera[8–11] (here, referred to as RSAS pressure).

Experimental determination of CSF compartmental pressures and flow is prohibitively difficult and invasive. The optic nerve SAS, in particular, is arguably the most important compartment in CSF-related ophthalmic diseases while simultaneously being one of the most difficult to experimentally access.[12–15] Therefore, investigations into the factors contributing to the role of TLPG in glaucoma should, at minimum, be based on the most important TLPG-governing variables derived from the first principles of fluid mechanics. To that end, the aim of this work is to identify patient-specific variables that contribute most significantly to RSAS pressure through a compartmental model that is consistent with first principles of fluid mechanics. In this paper, the "optic nerve SAS" refers to the entire SAS surrounding the optic nerve, while "RSAS" is the portion of the optic nerve SAS that is immediately posterior to the lamina cribrosa. The RSAS can be thought of as coinciding with the bulbar region which extends 3 mm behind the lamina cribrosa.

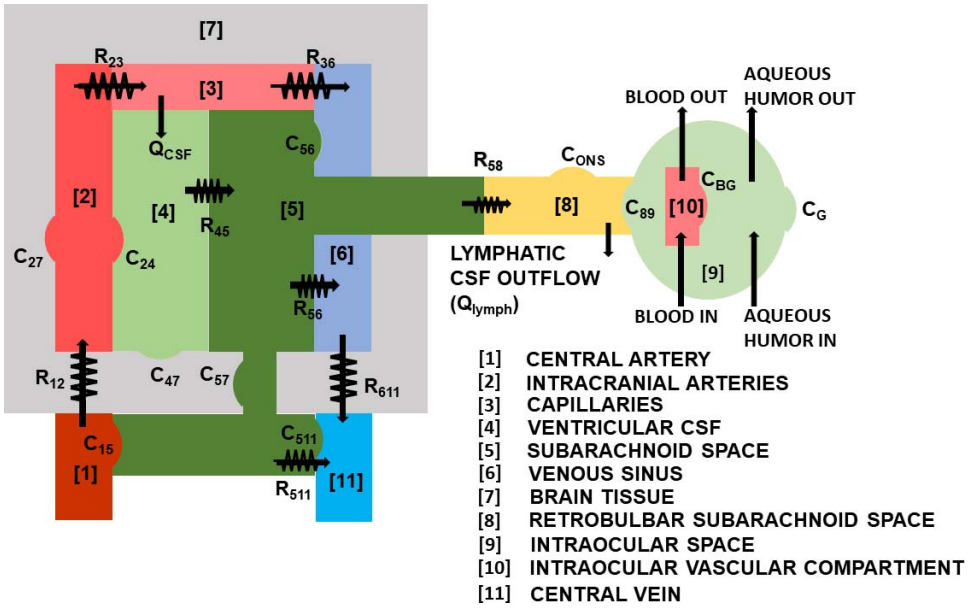

Figure 1. Schematic diagram of the 11-compartment model. The resistances are depicted by the distorted *arrows*. The *cup-shaped regions* represent the compliances.

Compartmental models have been used in the past to study intracranial dynamics, the effects of autoregulation, and for estimating model parameters (resistances and compliances).[16–22] Similarly, human eye compartmental models have been developed to investigate the relationship between the IOP and retinal hemodynamics[23] and the effect of altered cranial and systemic pressures due to gravitational changes on the IOP.[24] Recently, a three-dimensional pressure-dependent outflow model was proposed to estimate TLPG in the optic nerve head.[25] In the present study, an integrated compartmental model of the intracranial and intraocular dynamics is developed (Fig. 1), followed by a sensitivity analysis and parametric study designed to evaluate the role of individual parameters in RSAS pressure variation.

Methods

A schematic diagram of the developed compartmental model is shown in Figure 1. The intracranial and intraocular regions are divided into eleven compartments. The pressures in the compartments representing the central artery and the central vein act as the inputs for the mathematical model. The intracranial vascular compartments are lumped together into intracranial arteries, capillaries and venous sinus. The CSF circulation is described in a comprehensive review by Sakka et al.[26] The CSF flow is pulsatile and triggered by the systolic pulse wave in choroidal arteries, which are responsible for perfusing the choroid plexus for CSF production. This is represented in the model by the flow from the capillary compartment to the ventricular CSF compartment. In the SAS, the CSF circulates rostrally to the villous sites of absorption in the venous sinus or caudally to the spinal arachnoid villi. To differentiate the RSAS pressure from the lumped SAS pressure, a separate compartment for the optic nerve SAS is added. This is done because the size of the optic canal and the complex architecture within the optic nerve SAS contribute to a restriction in CSF flow, yielding an RSAS pressure that is different from the lumped SAS pressure. The intraocular space does not significantly exchange fluid with the adjacent RSAS,[27,28] but the IOP can be influenced through the deformation of the lamina cribrosa driven by the pressure difference between these compartments. Separate compartments for the vascular and aqueous humor are included to account for the change in the intraocular space volume corresponding to changes influenced by their dynamics within the eye. Mass balance equations are formulated for each compartment, resulting in a system of ordinary differential equations (ODEs) that describe the flow of blood and CSF within the model. The system of ODEs is solved using the built-in computing software (MATLAB ODE solver, ODE15S, MATLAB R2017b; MathWorks, Natick, MA, USA) to obtain the temporal variation of pressure in each compartment. Prior to solving the ODEs, it is necessary to establish model parameters. These parameters are primarily the lumped resistances between the compartments for pressure driven flows, and the compliances which relate volume changes to pressure changes. They are representative of anatomic features that act as flow restrictions or shared deformable boundaries, respectively.

Lumped parameter compartmental models are characterized by uniform pressure within each compartment. In the current model, all parameters are chosen based on the supine position; changes in position are not taken into account. All fluids are assumed to be incompressible and isothermal. The system of equations for the dependent variables (lumped compartmental pressures) is derived by applying the mass conservation law to each compartment. The rate of change of volume (dV/dt) is related to the fluid flowing in (Q_{in}) and flowing out (Q_{out}), as follows

$$\frac{dV}{dt} = Q_{in} - Q_{out} \quad (1)$$

Pressure driven flow for laminar fluids between two compartments is given by

$$Q_{ij} = \frac{P_i - P_j}{R_{ij}} \quad (2)$$

where Q_{ij} is the flow from the i^{th} compartment to the j^{th} compartment with the lumped resistance, R_{ij}, between the

two compartments. P_i and P_j are the lumped compartmental pressures. The change in the compartmental volume can also be represented using the compliance C_{ij} of the membrane separating the i^{th} and the j^{th} compartment. From symmetry one obtains the finding that $C_{ij} = C_{ji}$.

$$\frac{dV}{dt} = C_{ij}\frac{d(P_i - P_j)}{dt} \tag{3}$$

where $P_i - P_j$ represents the pressure difference across this membrane. Using Equations 1 through 3 yields the following system of equations of seven ODEs and one algebraic equation.

For the Intracranial Artery Compartment

$$C_{24}\frac{d(P_2 - P_4)}{dt} + C_{27}\frac{d(P_2 - P_7)}{dt} = \left(\frac{P_1}{R_{12}} - \frac{P_2}{R_{12}}\right) - \left(\frac{P_2}{R_{23}} - \frac{P_3}{R_{23}}\right) \tag{4}$$

Capillary Compartment

$$0 = \left(\frac{P_2}{R_{23}} - \frac{P_3}{R_{23}}\right) - \left(\frac{P_3}{R_{36}} - \frac{P_6}{R_{36}}\right) - Q_{CSF} \tag{5}$$

The capillary compartment is assumed to be nondeformable and hence the compliances between compartments 3 and 7, and 3 and 5 are not considered in the model.[18] A constant pressure difference is maintained between capillaries and the ventricular CSF (compartments 3 and 4) to maintain a constant production rate of CSF (Q_{CSF}).[21] Consequently, since there is no change in the pressure difference between these two compartments, the term $C_{34}\frac{d(P_3-P_4)}{dt}$ becomes zero. This reduces the left-hand side of Equation 5 to zero. Since the production rate of CSF is assumed to be independent of the pressure difference, it is not modeled as given by Equation 2, but rather considered as a constant.

Ventricular CSF Compartment

$$C_{24}\frac{d(P_4 - P_2)}{dt} + C_{47}\frac{d(P_4 - P_7)}{dt} = Q_{CSF} - \left(\frac{P_4}{R_{45}} - \frac{P_5}{R_{45}}\right) \tag{6}$$

SAS Compartment

$$C_{56}\frac{d(P_5 - P_6)}{dt} + C_{51}\frac{d(P_5 - P_1)}{dt} + C_{511}\frac{d(P_5 - P_{11})}{dt} + C_{57}\frac{d(P_5 - P_7)}{dt} = \left(\frac{P_4}{R_{45}} - \frac{P_5}{R_{45}}\right) - \left(\frac{P_5}{R_{56}} - \frac{P_6}{R_{56}}\right) - \left(\frac{P_5}{R_{511}} - \frac{P_{11}}{R_{511}}\right) - \left(\frac{P_5}{R_{58}} - \frac{P_8}{R_{58}}\right) \tag{7}$$

The central vein pressure (P_{11}) is assumed to be a constant value of 399.967 Pa (3 mm Hg)[22] and hence the corresponding derivative with respect to time is assumed to be negligible ($\frac{dP_{11}}{dt} \approx 0$).

Venous Sinus Compartment

$$C_{56}\frac{d(P_6 - P_5)}{dt} = \left(\frac{P_3}{R_{36}} - \frac{P_6}{R_{36}}\right) + \left(\frac{P_5}{R_{56}} - \frac{P_6}{R_{56}}\right) - \left(\frac{P_6}{R_{611}} - \frac{P_{11}}{R_{611}}\right) \tag{8}$$

Brain Tissue Compartment

$$C_{27}\frac{d(P_7 - P_2)}{dt} + C_{47}\frac{d(P_7 - P_4)}{dt} + C_{57}\frac{d(P_7 - P_5)}{dt} = 0 \tag{9}$$

RSAS Compartment

$$C_{ONS}\frac{d(P_8 - P_{OTP})}{dt} + C_{89}\frac{d(P_8 - P_9)}{dt} = \left(\frac{P_5}{R_{58}} - \frac{P_8}{R_{58}}\right) - Q_{lymph}$$

Assuming, $\frac{dP_{OTP}}{dt} \approx 0$,[29,30] gives

$$C_{ONS}\frac{dP_8}{dt} + C_{89}\frac{d(P_8 - P_9)}{dt} = \left(\frac{P_5}{R_{58}} - \frac{P_8}{R_{58}}\right) - Q_{lymph} \tag{10}$$

C_{ONS} is the compliance of the optic nerve sheath (ONS). The pressure outside the ONS is equivalent to the physiologic orbital tissue pressure (P_{OTP}) which is assumed to be a constant value.[29,30] This results in the derivative term associated with the orbital tissue pressure being negligible ($\frac{dP_{OTP}}{dt} \approx 0$). Q_{lymph} is the assumed lymphatic CSF outflow from the optic nerve SAS. Traditionally, it has been accepted that the majority of the CSF outflow takes place through the arachnoid granulations.[26] However, animal studies have suggested the possibility of CSF drainage through the lymphatic system.[31–42] Additionally, through histologic studies, Killer et al.[43] showed the presence of lymphatic capillaries in humans, predominantly located in the bulbar part of the optic nerve SAS.

Intraocular Compartment

The change in the intraocular compartment volume is formulated as outlined in Ref. 24 to obtain Equation 11. Detailed derivation is provided in the supplementary information.

$$C_{89}\frac{d(P_9 - P_8)}{dt} + C_{sbell}\frac{dP_9}{dt} + C_{bg}\frac{dP_9}{dt} - C_{ag}\frac{dP_{CRA}}{dt} - C_{vg}\frac{dP_{CRV}}{dt} = Q_{aq,in} - Q_{aq,out} \tag{11}$$

C_{sbell} is the compliance of the corneoscleral shell and the extraocular pressure, which is external to this membrane and is assumed to be constant. C_{bg} is defined as the total compliance of the intraocular vascular compartment with the globe. It can be formulated as the sum of the compliances associated with intraocular arteries (C_{ag}) and veins (C_{vg}) with the globe. P_{CRA} and P_{CRV} are the time varying central retinal artery and central retinal vein pressures, respectively, as shown in Figure 2. The waveforms for P_{CRA} and P_{CRV} at the control state are fitted using discrete Fourier series from the data given by Guidoboni et al.,[23] where the pressures are formulated through an inverse problem based on blood velocity measurements in the central retinal artery and central

retinal vein. The vascular system of the eye is far more complicated than just central retinal artery and vein pressures. The choroid, for example, represents an important contribution to ocular blood flow. However, due to the paucity of relevant literature, we have chosen to neglect the choroidal contribution within our model. $Q_{aq,in}$ is assumed to be constant while $Q_{aq,out}$ is a function of the aqueous outflow facility (C_{tm}), uveoscleral outflow rate (Q_{uv}), IOP and episcleral venous pressure (EVP).[24]

The system of seven ODEs given by Equations 4, 6 through 11, and one algebraic Equation 5, is reorganized as shown in Equation 12.

$$m(t,P)\frac{dP}{dt} = zP + f(t,P), \tag{12}$$

where $m(t,P), \frac{dP}{dt}, z, P$ and $f(t,P)$ are matrices which are shown below. The system of equations is numerically solved to evaluate compartmental pressures $P_2, P_3, P_4, P_5, P_6, P_7, P_8$, and P_9.

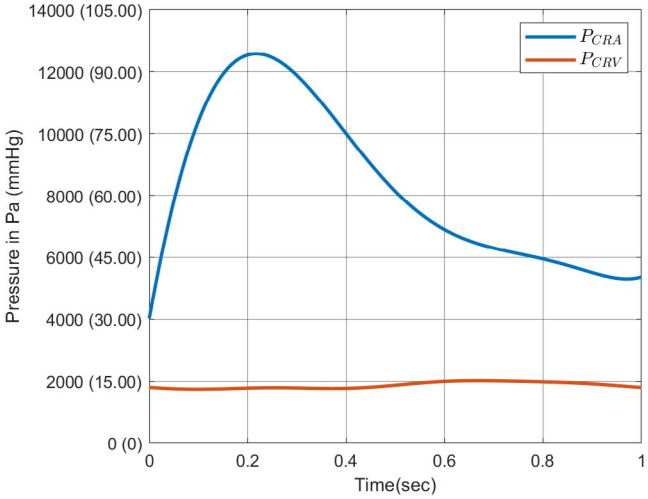

Figure 2. Time varying central retinal artery and central retinal vein pressure at the control state.

$$m(t,P) = \begin{bmatrix} C_{24}+C_{27} & 0 & -C_{24} & 0 & 0 & -C_{27} & 0 & 0 \\ 0 & 0 & 0 & 0 & 0 & 0 & 0 & 0 \\ -C_{24} & 0 & C_{24}+C_{47} & 0 & 0 & -C_{47} & 0 & 0 \\ 0 & 0 & 0 & C_{56}+C_{57}+C_{51}+C_{511} & -C_{56} & -C_{57} & 0 & 0 \\ 0 & 0 & 0 & -C_{56} & C_{56} & 0 & 0 & 0 \\ -C_{27} & 0 & -C_{47} & -C_{57} & 0 & C_{27}+C_{47}+C_{57} & 0 & 0 \\ 0 & 0 & 0 & 0 & 0 & 0 & C_{ONS}+C_{89} & -C_{89} \\ 0 & 0 & 0 & 0 & 0 & 0 & -C_{89} & C_{89}+C_{sbell}+C_{bg} \end{bmatrix}$$

$$\frac{dP}{dt} = \begin{bmatrix} \frac{dP_2}{dt} \\ \frac{dP_3}{dt} \\ \frac{dP_4}{dt} \\ \frac{dP_5}{dt} \\ \frac{dP_6}{dt} \\ \frac{dP_7}{dt} \\ \frac{dP_8}{dt} \\ \frac{dP_9}{dt} \end{bmatrix}, \quad \mathrm{P} = \begin{bmatrix} P_2 \\ P_3 \\ P_4 \\ P_5 \\ P_6 \\ P_7 \\ P_8 \\ P_9 \end{bmatrix}, \quad f(t,P) = \begin{bmatrix} \frac{P_1}{R_{12}} \\ -Q_{CSF} \\ Q_{CSF} \\ C_{51}\frac{dP_1}{dt} + \frac{P_{11}}{R_{511}} \\ \frac{P_{11}}{R_{611}} \\ 0 \\ -Q_{lympb} \\ Q_{aq,in} - (Q_{uv} - C_{tm}EVP) + C_{ag}\frac{dP_{CRA}}{dt} + C_{vg}\frac{dP_{CRV}}{dt} \end{bmatrix}$$

$$z = \begin{bmatrix} -\left(\frac{1}{R_{12}}+\frac{1}{R_{23}}\right) & \frac{1}{R_{23}} & 0 & 0 & 0 & 0 & 0 & 0 \\ \frac{1}{R_{23}} & -\left(\frac{1}{R_{23}}+\frac{1}{R_{36}}\right) & 0 & 0 & \frac{1}{R_{36}} & 0 & 0 & 0 \\ 0 & 0 & -\frac{1}{R_{45}} & \frac{1}{R_{45}} & 0 & 0 & 0 & 0 \\ 0 & 0 & \frac{1}{R_{45}} & -\left(\frac{1}{R_{45}}+\frac{1}{R_{56}}+\frac{1}{R_{58}}+\frac{1}{R_{511}}\right) & \frac{1}{R_{56}} & 0 & \frac{1}{R_{58}} & 0 \\ 0 & \frac{1}{R_{36}} & 0 & \frac{1}{R_{56}} & -\left(\frac{1}{R_{36}}+\frac{1}{R_{56}}+\frac{1}{R_{611}}\right) & 0 & 0 & 0 \\ 0 & 0 & 0 & 0 & 0 & 0 & 0 & 0 \\ 0 & 0 & 0 & \frac{1}{R_{58}} & 0 & 0 & -\frac{1}{R_{58}} & 0 \\ 0 & 0 & 0 & 0 & 0 & 0 & 0 & -C_{tm} \end{bmatrix}$$

Model Parameters

Resistances

All lumped resistance values, except for R_{58}, are calculated using Equation 2 by substituting the values of mean pressure and mean flow rate. The mean pressures and flow rates used in the model are summarized in Tables 1 and 2, respectively. Not all mean flow rates between compartments are known, therefore estimates were made under the assumption that the compartmental volumes remain constant at mean states.[18,21,44] This assumption implies that the mean inflow should equal the mean outflow for any particular compartment. Mean pressures for the intracranial compartments of an average human in the supine position are used for evaluating the intracranial resistances.[21] The central artery and central vein pressures are taken as inputs for the model. The central vein pressure is assumed to be a constant value of 399.967 Pa (3 mm Hg).[22] The central artery pressure signal given by Equation 13 and shown in Figure 3, was based on cine phase-contrast MRI measurements of a normal subject as enumerated by Linninger et al.[22]

Table 1. Mean Compartmental Pressures

Compartment	Mean Pressure in Pa (mm Hg)
Central artery ($\bar{P}_1$)	13.64×10^3 (102.34 mm Hg)[22]
Intracranial artery ($\bar{P}_2$)	10.67×10^3 (80 mm Hg)[21]
Capillaries ($\bar{P}_3$)	2.666×10^3 (20 mm Hg) [21]
Ventricular CSF ($\bar{P}_4$)	1.333×10^3 (10 mm Hg) [21]
SAS ($\bar{P}_5$)*	1.199×10^3 (9 mm Hg)[21]
Venous sinus ($\bar{P}_6$)	0.839×10^3 (6.3 mm Hg)[21]
Brain tissue ($\bar{P}_7$)	1.266×10^3 (9.5 mm Hg)[21]
Intraocular space ($\bar{P}_9$)	1.999×10^3 (15 mm Hg)[24]
Central vein ($\bar{P}_{11}$)	0.399×10^3 (3 mm Hg)[21]

* "SAS" in our paper corresponds to extraventricular space as it appears in Ref. 14.

$$P_1 = c_0[1 + \sum_{k=1}^{8} a_k \cos(\omega t) + \sum_{k=1}^{8} a_k \sin(\omega t)], \omega = 2k\pi, k = 1, 2, \ldots .8 \quad (13)$$

$$a_1, \ldots .a_8 = (-0.0345, -0.0511, -0.0267, -0.0111, -0.0013, 0.0050, 0.0027, 0.0061)$$

$$b_1, \ldots .b_8 = (0.1009, 0.0284, -0.0160, -0.0070, -0.0174, -0.0041, -0.0041, 0.0005)$$

$$c_0 = 102.353$$

The architecture of the optic nerve SAS has been shown to have numerous trabeculae, septae and pillars.[11,45,46] Based on the work of Killer et al.[46] as well as using the closed form solutions for permeability given by Westhuizen and Du Plessis,[47] the lumped resistance (R_{58}) offered to the CSF flow by this meshwork is estimated as follows. Since the mean flow rate of the CSF flowing into and out of the optic nerve SAS is not known, R_{58}, is estimated assuming the flow can be approximated as flow through a porous medium described by Darcy's law:

$$R = \frac{\mu L}{kA} \quad (14)$$

where μ is the viscosity of the CSF, L is the length over which the pressure drop occurs, k is the permeability and A is the area of cross-section of the optic nerve SAS. The viscosity of the CSF is assumed to be equal to that of water.[48,49] The length of the optic nerve SAS is reported to be 40 to 50 mm and is divided into four main regions: intraocular, midorbital, intracanalicular, and intracranial.[50–52] The cross-sectional area of each region is estimated from the optic nerve sheath diameter values reported at distances of 3, 9, and 15 mm behind the globe.[53] The optic nerve diameter and optic nerve sheath diameter values reported for the control group in Ref. 53 are used to estimate the area of cross-section within each region. Since the structure and density of the arachnoid trabeculae in the three segments varies,[45,46,54,55] the resistances for each segment were calculated separately based on their respective permeabilities. The permeability is estimated by assuming an idealized geometry wherein the trabeculae were considered to be straight cylindrical pillars, extending normally from the arachnoid layer to the pia layer.[48] This idealized representation of the SAS can be compared to a bed with unidirectional fibers, for which the analytical solutions for longitudinal and transverse permeability exist.[47] The longitudinal and transverse permeabilities for each of the three segments are calculated using Equations 15 and 16 and the corresponding resistance is calculated using Equation 14.

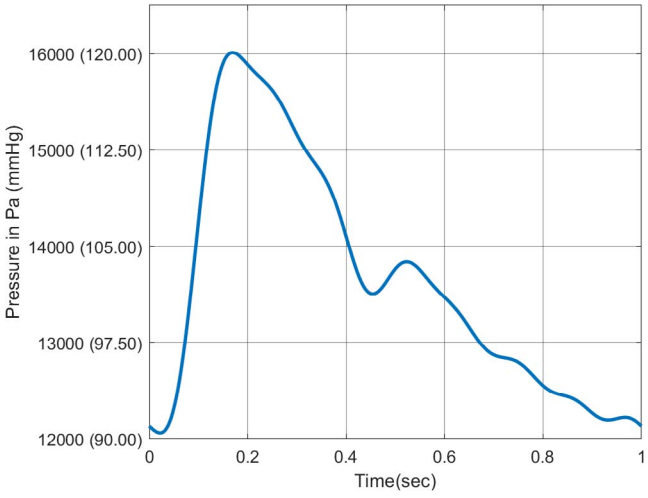

Figure 3. Central artery pressure signal which is the input pressure to the model.[22]

Table 2. Mean Compartmental Flows

Quantity	Mean Flow in m^3/s (ml/min)
$\bar{Q}_{12}, \bar{Q}_{611}$	Inflow and outflow equal to 1.250×10^{-5} (750 mL/min)[21]
Q_{CSF}	CSF production of 5.833×10^{-9} (0.35 mL/min)[21]
$\bar{Q}_{56}$	80% of total CSF outflow of 5.833×10^{-9} (0.35 mL/min)[21]
Q_{lymph}	Assumed to vary from 0% to 30% of total CSF outflow
$\bar{Q}_{511}$	Derived to match CSF outflow and inflow, $\bar{Q}_{511} = Q_{CSF} - \bar{Q}_{56} - Q_{lymph}$
$\bar{Q}_{45}$	Conserve compartment 4 volume, $\bar{Q}_{45} = Q_{CSF}$
$\bar{Q}_{23}$	Conserve compartment 2 volume, $\bar{Q}_{23} = \bar{Q}_{12}$
$\bar{Q}_{36}$	Conserve compartment 3 volume, $\bar{Q}_{36} = \bar{Q}_{23} - Q_{CSF}$

$$k_l = \frac{[\pi + 2.157(1-\varphi)]\varphi^2 r^2}{48(1-\varphi)^2} \quad (15)$$

$$k_t = \frac{\pi\varphi\left(1-\sqrt{\varphi}\right)^2 r^2}{24(1-\varphi)^{3/2}} \quad (16)$$

where k_l and k_t are the longitudinal and transverse permeabilities, respectively, φ is the porosity and r is the cross-sectional radius of the fibers. The porosity for the intracranial SAS is reported to be 0.99 in some studies.[48,56] However, since an exact value for the porosity of the optic nerve SAS is not known, the porosity is varied from 0.5–0.9. Based on the work of Killer et al.,[46] the bulbar region is characterized by round trabeculae with their profiles varying from 5 to 7 μm. An average diameter of 6 μm is assumed to estimate the resistance of this region. The midorbital region has large perforations interspersed with broad septae with an average diameter of 20 μm, while the intracanalicular region has mostly continuous SAS with pillars of approximately 25 μm diameter. Using the values for the anatomy of the optic nerve SAS and the radii of the trabeculae, septae and pillars, the resistance values for the three segments were estimated. Since the porosity values for each segment are not currently known, the lumped resistance (R_{58}) would not be a simple sum of the individual resistances of each segment at one particular porosity. Based on the histologic study carried out by Killer et al.[46] the porosity of the optic nerve SAS increases from the bulbar segment towards the

Investigative Ophthalmology & Visual Science

intracanalicular segment. Due to the difficulty associated with characterizing the porosity of each segment, R_{58} is varied from its possible estimated minimum value to its maximum value in order to see its effect on the resulting RSAS pressure. The minimum value of 6.752×10^9 Pa s/m^3 (0.844 mm Hg min/mL) is obtained by adding the longitudinal resistances at a porosity of 0.9 in all segments and similarly, the maximum value of 2.409×10^{12} Pa s/m^3 (301.162 mm Hg min/mL) is obtained by adding the transverse resistances at a porosity of 0.5.

Compliances

Compliance is the quantification of the ease with which a membrane separating two compartments deforms to allow an increase in the volume to accommodate an increase in pressure in either of the two compartments. The intracranial compliances are assumed to be constants, and are calculated using mean compartmental pressures.[21,57]

The lumped compliance of the ONS is located in the RSAS compartment as the sheath expansion is predominantly seen in the anterior portion, while the posterior portion exhibits smaller or even no discernible dilation.[29,54,55] The compliance associated with the ONS is estimated to be 4.283×10^{-12} m^3/Pa (0.571×10^{-3} mL/mm Hg) from an experimental study carried out by Hansen et al.[29] Optic nerve sheath diameter (ONSD) values at 3 mm distance from the lamina cribrosa, as reported in the study, were used to compute the corresponding change in volume over a length of 3 mm. The change in volume was then divided by the mean pressure difference corresponding to the ONSD changes in Ref. 29 to obtain the compliance of the ONS.

The compliance of the lamina cribrosa ($C_{98} = C_{89}$) between the optic nerve SAS and intraocular compartment is taken to be 8.251×10^{-15} m^3/Pa (1.1×10^{-6} mL/mm Hg).[24] As outlined in Ref. 24, the summation of the compliance of the lamina cribrosa (C_{98}), the compliance of the corneoscleral shell (C_{sbell}) and the compliance of the intraocular vascular compartment with the globe (C_{bg}), can be considered as the in vivo globe compliance ($C_{g,invivo}$). Thus, $C_{g,invivo} = C_{98} + C_{sbell} + C_{bg}$ can be substituted in $m(t,P)$, where $C_{g,invivo}$ is included in the model as given by Equation 17.

$$C_{g,invivo} = V_{g0}\left(\frac{C_1}{P_9} + C_2\right) \tag{17}$$

where V_{g0} is the average globe starting volume, considered to be 6.500×10^{-6} m^3 (6.5 mL) and C_1 and C_2 are empirical constants 4.87×10^{-3} and 2.925×10^{-7} Pa^{-1} (3.9×10^{-5} mm Hg^{-1}), respectively.

The compliance C_{bg} can be separated into its respective arterial (C_{ag}) and venous compliance (C_{vg}) using a factor $\omega = 0.7$. The C_{ag} is assumed to be constant with respect to changing IOP (P_9), while C_{vg} is a function of IOP (P_9) and are calculated using Equation 18.[24]

$$C_{ag} = (1-\omega)C_{bg0}$$

$$C_{vg0} = \omega C_{bg0}$$

and

$$C_{vg} = C_{vg0} + \Delta C_{bg}$$

$$\text{where } C_{bg0} = V_{g0}\left(\frac{C_1}{P_9} + C_2 - \frac{1}{kP_9}\right) \tag{18}$$

assuming normal IOP, $P_9 = 2.000 \times 10^3$ Pa (15 mm Hg) and the nondimensional globe stiffness, $k = 312$.

Table 3. Baselines for Parameterized Variables

Parameter	Value
R_{12}	2.383×10^8 Pa s/m^3 (0.0298 mm Hg/mL/min)[21]
R_{23}	6.399×10^8 Pa s/m^3 (0.080 mm Hg/mL/min)[21]
R_{36}	1.462×10^8 Pa s/m^3 (0.0183 mm Hg/mL/min)[21]
R_{45}	2.286×10^{10} Pa s/m^3 (2.8571 mm Hg/mL/min)[21]
R_{56}	7.714×10^{10} Pa s/m^3 (9.6429 mm Hg/mL/min)[21]
R_{511}	1.371×10^{12} Pa s/m^3 (85.7143 mm Hg/mL/min)[21]
R_{611}	3.520×10^7 Pa s/m^3 (0.0044 mm Hg/mL/min)[21]
R_{58}	1.688×10^{12} Pa s/m^3 (210.983 mm Hg min/mL)*
C_{27}	1.572×10^{-10} m^3/Pa (0.0209523 mL/mm Hg)[21]
C_{24}	1.965×10^{-10} m^3/Pa (0.0261999 mL/mm Hg)[21]
C_{47}	2.719×10^{-10} m^3/Pa (0.036255 mL/mm Hg)[21]
C_{56}	9.573×10^{-9} m^3/Pa (1.27626 mL/mm Hg)[21]
C_{57}	1.028×10^{-9} m^3/Pa (0.137057 mL/mm Hg)[21]
C_{51}	4.286×10^{-11} m^3/Pa (0.00571427 mL/mm Hg)[21]
C_{511}	1.507×10^{-9} m^3/Pa (0.200936 mL/mm Hg)[21]
C_{ONS}	4.283×10^{-12} m^3/Pa (0.000571 mL/mm Hg)[29]
C_{89}	8.251×10^{-15} m^3/Pa (1.1×10^{-6} mL/mm Hg)[24]
C_1	3.653×10^{-5} Pa^{-1} (4.87×10^{-3} mm Hg^{-1})[24]
C_2	2.925×10^{-7} Pa^{-1} ($3.9 \times$ x10^{-5} mm Hg^{-1})[24]
V_{g0}	6.500×10^{-6} m^3 (6.5 mL)[24]
ω	0.7[24]
k	312[24] (Non-dimensional globe stiffness)
C_{tm}	3.750×10^{-14} m^3/s Pa (0.3×10^{-3} mL/min mm Hg)[24]
$Q_{aq,in}$	4.000×10^{-11} m^3/s (2.4×10^{-3} mL/min)[24]
Q_{uv}	6.667×10^{-12} m^3/s (0.4×10^{-3} mL/min)[24]
Q_{CSF}	5.833×10^{-9} m^3/s (0.35 mL/min)[21]
Q_{lymph}	4.667×10^{-10} m^3/s (0.028 mL/min)†
EVP	933.254 Pa (7 mm Hg)[24]

* The range for R_{58} is estimated as highlighted in the section on Resistance under Model Parameters. The above value for R_{58} in conjunction with Q_{lymph} generated RSAS pressures reported by Liu and Kahn.[11]

† The above value for Q_{lymph} is estimated based on qualitative evidence[37–42] and such that it generated RSAS pressures reported by Liu and Kahn,[11] which is discussed in detail in the "Results" section.

Results

A sensitivity analysis of the model was carried out to determine how each of the 28 parameters, which are summarized in Table 3, affect the RSAS pressure. The method outlined by Huson[58] was followed with minor adjustments to determine the most sensitive parameters. Since physiologic data for some of the parameters, especially those associated with the optic nerve SAS, are unknown, the analysis incorporates the assumption that uncertainty about the baseline parameter values is represented by uniform distributions, with a range of ± 30% of the baseline value.[59] Latin hypercube sampling was used to take samples of each parameter individually. A total of 1000 samples of each of the 28 parameters were generated, such that the sample size was much larger than the number of parameters, to ensure accuracy.[59] Sensitivity coefficients of 5%, as described by Huson,[58] were calculated for all eight output compartmental pressures with respect to each of the parameters. The values of the 5% sensitivity coefficients are bounded by 0 and 1, with a higher value indicating that a greater proportion of the generated output pressures lie outside the range of ± 5% of the corresponding mean pressure value. The RSAS pressure is affected by R_{12}, R_{23}, R_{611}, R_{58}, and Q_{lymph} with the 5% sensitivity coefficients for each being 0.44, 0.53, 0.77, 0.89, and 0.90, respectively.

A local sensitivity analysis was further carried out to compute the sensitivity coefficients in order to determine the effect of the above five parameters on the RSAS pressure. The

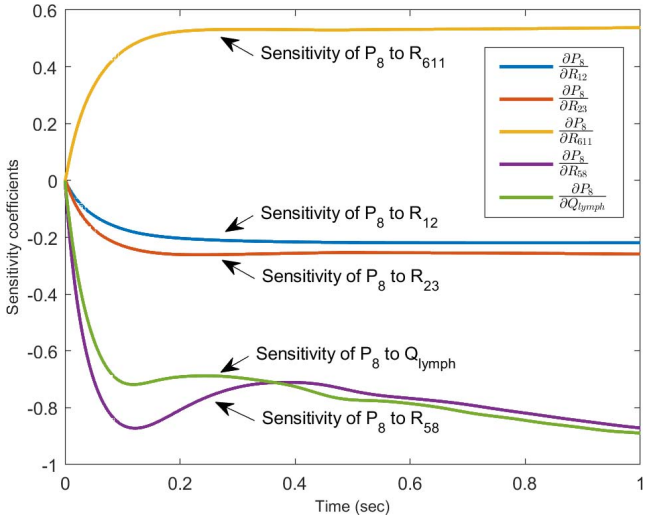

Figure 4. Sensitivity coefficients for effect of R_{12}, R_{23}, R_{611}, R_{58}, and Q_{lymph} on RSAS pressure P_8.

sensitivity coefficients in Figure 3 were computed by the finite difference approximation.[60] Similar graphs were generated for other parameters which are included in the supplementary information. R_{12}, R_{23}, R_{611}, R_{58}, and Q_{lymph} were identified as the parameters that affected the RSAS pressure the most, which is consistent with the results obtained from the method outlined by Huson.[58] Figure 4 shows that the RSAS pressure is most sensitive to the optic nerve SAS resistance (R_{58}) and the lymphatic CSF outflow (Q_{lymph}) through this space.

It was observed that in certain animals, such as cats and rabbits, up to 30% of CSF drains out through two major lymphatic pathways; one in the olfactory bulb and the other in the optic nerve SAS.[36,61] However, due to the lack of an estimate for the portion of CSF which is draining out through the lymphatic system in the optic nerve SAS of humans, all potential outflow cases are investigated in this study. The assumed values range from 0% to 30% of the total CSF outflow in order to span the entire range of possibilities currently reported in the literature; ranging from no lymphatic CSF outflow to the entire outflow from the optic nerve SAS only. A parametric study was carried out by varying the optic nerve SAS resistance (R_{58}) from 6.752×10^9 Pa s/m^3 (0.844 mm Hg min/mL) to 2.409×10^{12} Pa s/m^3 (301.162 mm Hg min/mL), and the lymphatic outflow of the CSF from this region from 0% to 30% of the CSF outflow. This was done to investigate the resulting effects on the RSAS pressure and capture both limiting cases (the two extreme values of the parameters) of this mechanism. The resulting time-averaged RSAS pressure values are plotted as a surface plot in Figure 5. The RSAS pressure values reported by Liu and Kahn[11] varied from 0 to 800.0 Pa (0–6 mm Hg). It can be seen from Figure 5 that the RSAS pressures over all ranges of resistances are greater than the maximum reported value of 800.0 Pa (6 mm Hg) when there is no lymphatic CSF outflow from the optic nerve SAS. This fluid mechanics-based observation supports the study carried out by Killer et al.[62] who found evidence of lymphatic capillaries in the dura of the human optic nerve, suggesting the existence of some amount of lymphatic CSF drainage from the optic nerve SAS. In the scenario for no

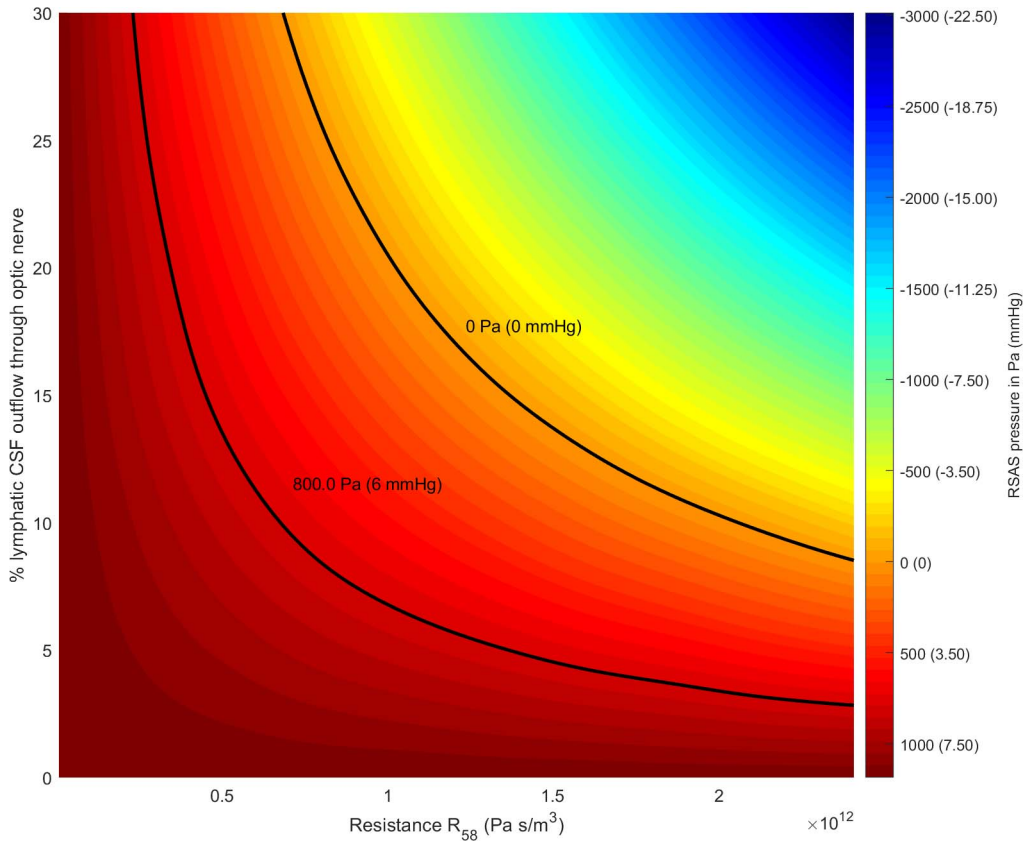

Figure 5. Surface plot of the mean RSAS pressure values for varying resistance and outflow conditions.

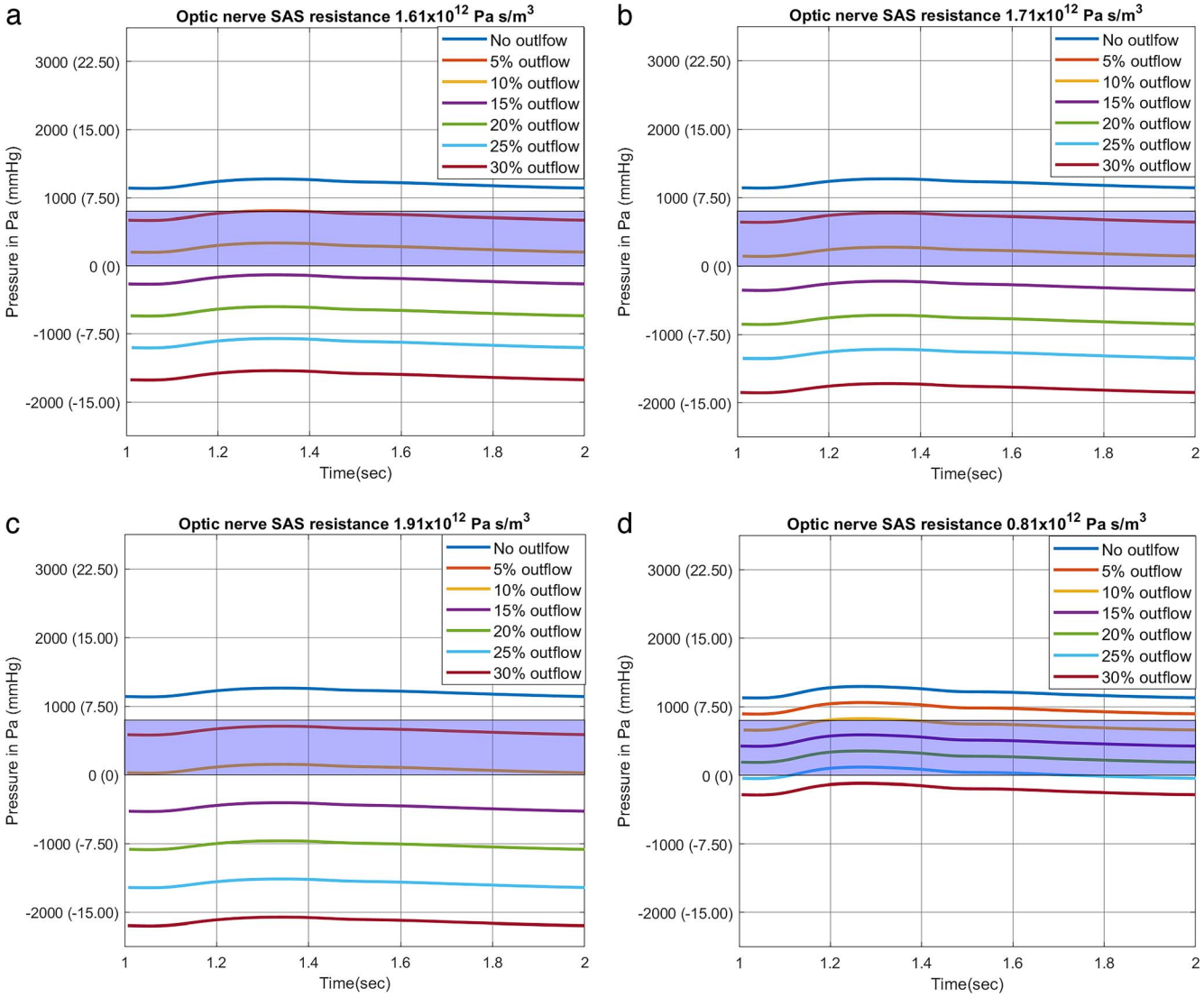

Figure 6. (**a**) RSAS pressure variation for different outflow conditions at optic nerve SAS resistance of 1.61×10^{12} Pa s/m3 (201.3 mm Hg min/mL). (**b**) RSAS pressure variation for different outflow conditions at optic nerve SAS resistance of 1.71×10^{12} Pa s/m3 (213.8 mm Hg min/mL). (**c**) RSAS pressure variation for different outflow conditions at optic nerve SAS resistance of 1.91×10^{12} Pa s/m3 (238.7 mm Hg min/mL) (**d**) RSAS pressure variation for different outflow conditions at optic nerve SAS resistance of 0.81×10^{12} Pa s/m3 (101.3 mm Hg min/mL).

lymphatic CSF outflow, the possibility of CSF moving out of the RSAS into the SAS is accounted for in the model. This movement of CSF depends on the direction of the pressure gradient between the RSAS and SAS compartments and a detailed explanation is provided in the supplementary information.

Figure 6 shows the variation in RSAS pressure for different CSF outflow conditions at a particular optic nerve SAS resistance. Figures 6A through 6C illustrate that for the particular resistances, the RSAS pressures lie within the reported range of 0 to 800.0 Pa (0–6 mm Hg[11]; shaded region) only for lymphatic CSF outflows of 5% to 10% through the optic nerve SAS. For the remaining outflow conditions, where the CSF outflow through the lymphatics in the optic nerve is less than 5% or greater than 10%, the RSAS pressures lie outside the reported range of values. This relatively small percentage of CSF outflow through the optic nerve lymphatic network is consistent with the numerous animal studies favoring the nasal lymphatics as the more significant outflow path.[37–42,62,63] Moreover, outflow tracts into the human lymphatic networks in the submucosa associated with the nasal epithelium have also been established.[64] Based on the extensive literature, the bulk of the CSF drainage seems to take place through the nasal rather than optic nerve lymphatics.[62,63] In contrast, Figure 6d illustrates that for a lower resistance, the majority of the CSF outflow (10%–25%) must be through the lymphatics in the optic nerve for the RSAS pressures to lie within the reported range (shaded region). This indicates that for a lower value of the resistance in this area, the RSAS pressures are consistent with the reported values, albeit with an increased CSF outflow through the lymphatics. This higher percentage of CSF outflow (10%–25%) through the optic nerve lymphatics required in such a scenario is contrary to the extensive experimental evidence that suggests that the nasal lymphatics are the primary outflow tract.[37–42,62,63] Additional figures for the entire range of resistances are included in the supplemental information.

Although RSAS pressure is likely the most important compartmental pressure with respect to CSF-related ophthalmic disease, for completeness all compartmental pressures

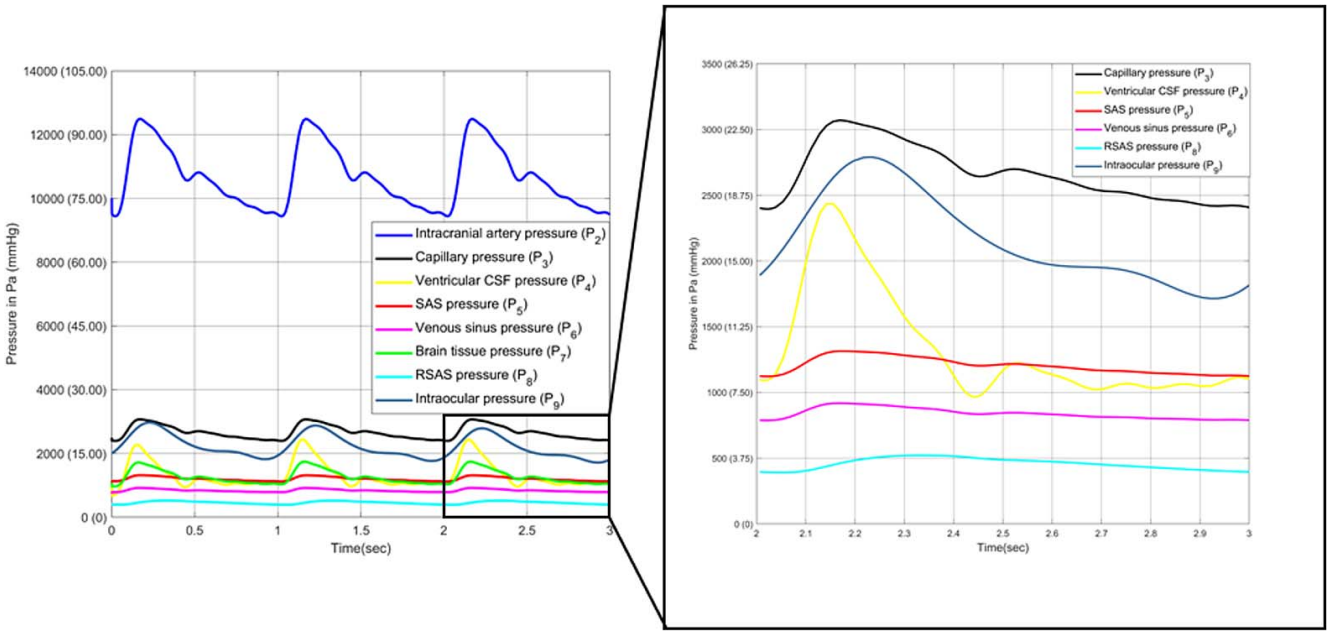

Figure 7. Temporal variation in compartmental pressures.

were considered in our model. For example, temporal variations in compartmental pressures are shown in Figure 7 for a resistance of 1.909×10^{12} Pa s/m^3 (238.6 mm Hg min/mL) and 7% lymphatic CSF outflow through the optic nerve SAS, which results in a mean RSAS pressure of close to 400.0 Pa (3 mm Hg). Moreover, the predicted values of IOP and ICP matched well with those reported by Eklund et al.[65] The mean IOP as predicted by the model is 2187.82 Pa (16.41 mm Hg), which matches well with the clinically observed mean IOP of 2293.15 Pa (17.2 mm Hg). The model does not consider the hydrostatic effects, however, the IOP at the level of the lamina cribrosa reported in the study is only slightly different at 2519.80 Pa (18.9 mm Hg). The study reports mean ICP at the level of the lamina cribrosa to be 879.93 Pa (6.6 mm Hg). It is estimated from the ICP measured through a lumbar puncture by factoring the hydrostatic effects. The model, on the other hand, predicts a range of mean RSAS pressure (CSF pressure at the level of lamina cribrosa) from 1105.24 Pa (8.29 mm Hg) to 422.63 Pa (3.17 mm Hg), depending on a range of 0% to 7% of lymphatic CSF outflow, respectively, with the resistance of the optic nerve SAS of 1.909×10^{12} Pa s/m^3 (238.6 mm Hg min/mL). The model predicts about 2.3% lymphatic CSF outflow with a similar resistance for the mean RSAS pressure to match the mean ICP at the level of the lamina cribrosa (879.93 Pa [6.6 mm Hg]), as reported in the study. Central artery pressure is not correlated with the intracranial CSF pressure.[66] The model is consistent with the literature in this regard. For example, increasing the input central artery pressure (P_1) by 30% increased the SAS pressure (P_5) only marginally, by 0.6%.

Conclusions

The intent of this study was to identify the primary factors governing RSAS pressure through an integrated compartmental model describing the intracranial, vascular and intraocular dynamics. The RSAS pressure directly affects TLPG, which is hypothesized to play a role in the development of glaucoma. A sensitivity analysis revealed that the RSAS pressure is most affected by two variables: flow resistance in the optic nerve SAS (R_{58}) and the outflow of CSF (Q_{lympb}) from this space through the lymphatic system. Based on the results of the sensitivity analysis, a parametric study was performed to evaluate the effect of different optic nerve SAS resistances and outflow conditions on the RSAS pressure. Due to the complexity of the optic nerve SAS architecture, cross-sectional area variations, and potential flow restriction offered by the optic canal, the optic nerve SAS resistance is likely to vary considerably from person to person. It was observed that when there was no lymphatic outflow of CSF, the model consistently predicted higher RSAS pressure values than those reported in literature,[11] over the entire range of physiologically reasonable resistances. This observation suggested that modest CSF outflow through the lymphatic system in the optic nerve is likely, as reported by other researchers.[62] Resistance in the range of 1.600×10^{12} Pa s/m^3 (201.1 mm Hg min/ml) to 1.909×10^{12} Pa s/m^3 (238.6 mm Hg min/mL), and lymphatic CSF outflow in the range of 5% to 10% were required to generate RSAS pressures consistent with fluid mechanics and with RSAS pressure ranges reported in the literature. These results highlight the clinical relevance of lymphatic outflow in this region and the flow resistance between the intracranial and RSAS compartment. The results further suggest that any person-to-person variation in these variables should be an important consideration in investigations of TLPG-related mechanisms of glaucoma development.

The proposed model has a number of limitations. The model is linear and assumes constant compliances and resistances. Additionally, all the parameters used in the model are valid for humans in supine position and do not take into account the effect of posture on the pressures, and the flow of blood and CSF in the body. Linear compartmental models[18,22] assuming supine conditions for all baseline parameters have been developed in the past.[21] While this linear model does not describe complex phenomena such as autoregulation or consider the effects of posture, it does provide a useful method to investigate the parameters that affect the TLPG and their relative importance. Additionally, there are various limitations associated with the cadaver study referenced for the reported values of RSAS pressure.[11] Among the issues that may limit the extrapolation of experimental parameters in the cadaver study to the general, living population are: the lack of respiration, the

freshness of the cadavers and the associated effects on tissue properties, and the inability to confidently define average optic nerve space characteristics due to the limited number of cadavers used. These limitations are partially mitigated in the proposed model by using a range of parameter values that generate RSAS pressures not limited to those reported in the cadaver study. Additionally, the model is not configured to incorporate artificially induced variation in other compartment pressures such as ventricles. Hence, a direct comparison with the results of living animal studies,[8,10] correlating the ventricular pressure to the RSAS pressure is not possible. Currently, there are limited experimental studies that give reliable estimates of the physiologic parameters for the critical optic nerve SAS. The lack of reliable experimental measurements and the difficulty associated with experimental characterization of brain tissue is a challenge faced by all mathematical models of this type, and a primary reason for their necessity. The accuracy of the model would be substantially improved with the addition of reliable experimental characterization of a physiologic baseline for parameters such as the porosity of the optic nerve SAS, compliance of the ONS, or the proportion of CSF outflow through the lymphatics in the optic nerve. This is reflected in the sensitivity analysis, where the parameters were varied individually, although there is a chance that they may be dependent on each other. This approach, while based on several simplifications and assumptions, permits the identification of parameters critical to the RSAS pressure with considerable confidence. In addition to the insights derived from the model's behavior, the relative importance of each parameter may serve to inform the direction and focus of future experimental studies and, subsequently, the development of more complex and physiologically accurate models.

Acknowledgments

Supported by the National Center for Advancing Translational Sciences (NCATS), National Institutes of Health, through Grant Award Number UL1TR002489. The content is solely the responsibility of the authors and does not necessarily represent the official views of the NIH. Additionally, the project was supported by the 2015 American Glaucoma Society MAPS Award, 2017 American Glaucoma Society Young-Clinician Scientist Award, 2017 Chandler-Grant Society Award, and 2017 UNC University Research Council grant.

Disclosure: **O.G. Kaskar**, None; **D. Fleischman**, None; **Y.Z. Lee**, None; **B.D. Thorp**, None; **A.V. Kuznetsov**, None; **L. Grace**, None

References

1. Quigley HA, Broman AT. The number of people with glaucoma worldwide in 2010 and 2020. *Br J Ophthalmol*. 2006;90:262–267.
2. Klein BE, Klein R, Sponsel WE, et al. Prevalence of glaucoma: The beaver dam eye study. *Ophthalmology*. 1992;99:1499–1504.
3. Bonomi L, Marchini G, Marraffa M, et al. Prevalence of glaucoma and intraocular pressure distribution in a defined population: The Egna-Neumarkt study. *Ophthalmology*. 1998;105:209–215.
4. Harada T, Harada C, Nakamura K, et al. The potential role of glutamate transporters in the pathogenesis of normal tension glaucoma. *J Clin Invest*. 2007;117:1763–1770.
5. Berdahl JP, Allingham RR, Johnson DH. Cerebrospinal fluid pressure is decreased in primary open-angle glaucoma. *Ophthalmology*. 2008;115:763–768.
6. Ren R, Jonas JB, Tian G, et al. Cerebrospinal fluid pressure in glaucoma: A prospective study. *Ophthalmology*. 2010;117:259–266.
7. Berdahl JP, Allingham RR. Intracranial pressure and glaucoma. *Curr Opin Ophthalmol*. 2010;21:106–111.
8. Hou R, Zhang Z, Yang D, et al. Intracranial pressure (ICP) and optic nerve subarachnoid space pressure (ONSP) correlation in the optic nerve chamber: The Beijing intracranial and intraocular pressure (iCOP) study. *Brain Res*. 2016;1635:201–208.
9. Morgan WH, Yu D, Cooper RL, Alder VA, Cringle SJ, Constable IJ. The influence of cerebrospinal fluid pressure on the lamina cribrosa tissue pressure gradient. *Invest Ophthalmol Vis Sci*. 1995;36:1163–1172.
10. Morgan WH, Yu D, Alder VA, et al. The correlation between cerebrospinal fluid pressure and retrolaminar tissue pressure. *Invest Ophthalmol Vis Sci*. 1998;39:1419–1428.
11. Liu D, Kahn M. Measurement and relationship of subarachnoid pressure of the optic nerve to intracranial pressures in fresh cadavers. *Am J Ophthalmol*. 1993;116:548–556.
12. Killer HE, Jaggi GP, Flammer J, Miller NR, Huber AR. The optic nerve: a new window into cerebrospinal fluid composition? *Brain*. 2006;129:1027–1030.
13. Killer HE, Jaggi GP, Miller NR. Papilledema revisited: is its pathophysiology really understood? *Clin Experiment Ophthalmol*. 2009;37:444–447.
14. Killer HE, Pircher A. Normal tension glaucoma: review of current understanding and mechanisms of the pathogenesis. *Eye (Lond)*. 2018;32:924–930.
15. Killer HE, Jaggi GP, Flammer J, Miller NR. Is open-angle glaucoma caused by impaired cerebrospinal fluid circulation: Around the optic nerve? *Clin Experiment Ophthalmol*. 2008;36:308–311.
16. Monro A. Observations on the structure and functions of the nervous system. *Lond Med J*. 1783;4:113–135.
17. Kellie G. An account with some reflections on the pathology of the brain. *Edinburgh Med Chir Soc Trans*. 1824;1:84–169.
18. Karni Z, Bear J, Sorek S, Pinczewski Z. Quasi-steady-state compartmental model of intracranial fluid dynamics. *Med Biol Eng Comput*. 1987;25:167–172.
19. Sorek S, Bear J, Karni Z. A non-steady compartmental flow model of the cerebrovascular system. *J Biomech*. 1988;21:695–704.
20. Lakin WD, Yu J, Penar PL, Kadas ZM. A mathematical model of the intracranial system including autoregulation. *Neurol Res*. 1997;19:441–450.
21. Lakin WD, Stevens SA, Tranmer BI, Penar PL. A whole-body mathematical model for intracranial pressure dynamics. *J Math Biol*. 2003;46:347–383.
22. Linninger A, Sweetman B, Penn R. A mathematical model of blood, cerebrospinal fluid and brain dynamics in communicating hydrocephalus. *Clin Neurol Neurosurg*. 2008;110:S4.
23. Guidoboni G, Harris A, Cassani S, et al. Intraocular pressure, blood pressure, and retinal blood flow autoregulation: A mathematical model to clarify their relationship and clinical relevance. *Invest Ophthalmol Vis Sci*. 2014;55:4105–4118.
24. Nelson ES, Mulugeta L, Feola A, et al. The impact of ocular hemodynamics and intracranial pressure on intraocular pressure during acute gravitational changes. *J Appl Physiol*. 2017;123:352.
25. Smith DW, Lee C, Morgan W, Gardiner BS. Estimating three-dimensional outflow and pressure gradients within the human eye. *PLoS One*. 2019;14:e0214961.
26. Sakka L, Coll G, Chazal J. Anatomy and physiology of cerebrospinal fluid. *Eur Ann Otorhinolaryngol Head Neck Dis*. 2011;128:309–316.
27. Cebula H, Kremer S, Chibbaro S, Proust F, Bierry G. Subarachnoidal migration of intraocular silicone oil. *Acta Neurochir*. 2017;159:347.

28. Wostyn P, De Groot V, Van Dam D, Audenaert K, Killer HE, De Deyn PP. Evidence for the existence of a communication between the eye and the brain? *Acta Neurochir*. 2017;159: 1413–1414.
29. Hansen H, Lagrèze W, Krueger O, Helmke K. Dependence of the optic nerve sheath diameter on acutely applied subarachnoidal pressure–an experimental ultrasound study. *Acta Ophthalmol*. 2011;89:e532.
30. Moller PM. The pressure in the orbit. *Acta Ophthalmol Suppl*. 1955:1–100.
31. Johnston M. Relationship between cerebrospinal fluid and extracranial lymph. *Lymphology*. 2000;33:1–3.
32. Johnston M. The importance of lymphatics in cerebrospinal fluid transport. *Lymphat Res Biol*. 2003;1:41–45.
33. Zakharov A, Papaiconomou C, Djenic J, Midha R, Johnston M. Lymphatic cerebrospinal fluid absorption pathways in neonatal sheep revealed by subarachnoid injection of Microfil. *Neuropathol Appl Neurobiol*. 2003;29:563–573.
34. Erlich SS, McComb JG, Hyman S, Weiss MH. Ultrastructure of the orbital pathway for cerebrospinal fluid drainage in rabbits. *J Neurosurg*. 1989;70:926–931.
35. McComb JG, Hyman S. Lymphatic drainage of cerebrospinal fluid in the primate. In: Johansson BB, Widner H, eds. *Pathophysiology of the Blood-Brain Barrier*. New York, NY: Elsevier Science Publishers. 1990:421–437.
36. Bradbury MW, Cole DF. The role of the lymphatic system in drainage of cerebrospinal fluid and aqueous humour. *J Physiol (Lond)*. 1980;299:353–365.
37. Boulton M, Yonung A, Hay J, et al. Drainage of CSF through lymphatic pathways and arachnoid villi in sheep: Measurement of 125I-albumin clearance. *Neuropathol Appl Neurobiol*. 1996;22:325–333.
38. Boulton M, Armstrong D, Flessner M, Hay J, Szalai JP, Johnston M. Raised intracranial pressure increases CSF drainage through arachnoid villi and extracranial lymphatics. *Am J Physiol*. 1998;275:R896.
39. Boulton M, Flessner M, Armstrong D, Hay J, Johnston M. Determination of volumetric cerebrospinal fluid absorption into extracranial lymphatics in sheep. *Am J Physiol*. 1998; 274:R96.
40. Boulton M, Flessner M, Armstrong D, Mohamed R, Hay J, Johnston M. Contribution of extracranial lymphatics and arachnoid villi to the clearance of a CSF tracer in the rat. *Am J Physiol*. 1999;276:R823.
41. Papaiconomou C, Zakharov A, Azizi N, Djenic J, Johnston M. Reassessment of the pathways responsible for cerebrospinal fluid absorption in the neonate. *Childs Nerv Syst*. 2004;20: 29–36.
42. Zakharov A, Papaiconomou C, Koh L, Djenic J, Bozanovic-Sosic R, Johnston M. Integrating the roles of extracranial lymphatics and intracranial veins in cerebrospinal fluid absorption in sheep. *Microvasc Res*. 2004;67:96–104.
43. Killer HE, Laeng HR, Groscurth P. Lymphatic capillaries in the meninges of the human optic nerve. *J Neuroophthalmol*. 1999;19:222–228.
44. Stevens SA, Lakin WD, Penar PL. Modeling steady-state intracranial pressures in supine, head-down tilt and microgravity conditions. *Aviat Space Environ Med*. 2005;76:329–338.
45. Hayreh SS. Pathogenesis of oedema of the optic disc (papilloedema): a preliminary report. *Br J Ophthalmol*. 1964;48:522.
46. Killer HE, Laeng HR, Flammer J, Groscurth P. Architecture of arachnoid trabeculae, pillars, and septa in the subarachnoid space of the human optic nerve: anatomy and clinical considerations. *Br J Ophthalmol*. 2003;87:777–781.
47. Westhuizen J, Du Plessis JP. Quantification of unidirectional fiber bed permeability. *J Composite Mater*. 1994;28:619–637.
48. Kurtcuoglu V, Soellinger M, Boesiger P, Poulikakos D, Gupta S. Three-dimensional computational modeling of subject-specific cerebrospinal fluid flow in the subarachnoid space. *J Biomech Eng*. 2009;131:021010.
49. Sweetman B, Xenos M, Zitella L, Linninger AA. Three-dimensional computational prediction of cerebrospinal fluid flow in the human brain. *Comput Biol Med*. 2010;41:67–75.
50. Pircher A, Montali M, Wostyn P, et al. Impaired cerebrospinal fluid dynamics along the entire optic nerve in normal-tension glaucoma. *Acta Ophthalmol*. 2018;96:e562–e569.
51. Duke-Elder S. *System of Ophthalmology: The Anatomy of the Visual System*. Vol 2. St. Louis, MO: Kimpton; 1961.
52. Treuting PM, Frevert CW, Liggitt D, Dintzis SM. *Comparative Anatomy and Histology: A Mouse, Rat, and Human Atlas*. San Diego, CA: Elsevier Science & Technology; 2011.
53. Wang N, Xie X, Yang D, et al. Orbital cerebrospinal fluid space in glaucoma: the Beijing intracranial and intraocular pressure (iCOP) study. *Ophthalmology*. 2012;119:2073. e1.
54. Hansen HC, Helmke K. The subarachnoid space surrounding the optic nerves. An ultrasound study of the optic nerve sheath. *Surg Radiol Anat*. 1996;18:323–328.
55. Soldatos T, Chatzimichail K, Papathanasiou M, Gouliamos A. Optic nerve sonography: a new window for the non-invasive evaluation of intracranial pressure in brain injury. *Emerg Med J*. 2009;26:630–634.
56. Tada Y, Nagashima T. Modeling and simulation of brain lesions by the finite-element method. *IEEE Eng Med Biol Mag*. 1994; 13:497–503.
57. Stevens SA, Lakin WD. Local compliance effects on the global pressure-volume relationship in models of intracranial pressure dynamics. *Math Comput Model Dyn Syst*. 2000;6:445–465.
58. Huson LW. Definition and properties of a coefficient of sensitivity for mathematical models. *Ecol Model*. 1984;21: 149–159.
59. Marino S, Hogue IB, Ray CJ, Kirschner DE. A methodology for performing global uncertainty and sensitivity analysis in systems biology. *J Theor Biol*. 2008;254:178–196.
60. Zi Z. Sensitivity analysis approaches applied to systems biology models. *IET systems biology*. 2011;5:336–346.
61. Morgan WH, Balaratnasingam C, Lind CR, et al. Cerebrospinal fluid pressure and the eye. *Br J Ophthalmol*. 2016;100:71–77.
62. Killer HE, Laeng HR, Groscurth P. Lymphatic capillaries in the meninges of the human optic nerve. *J Neuroophthalmol*. 1999;19:222–228.
63. Brinker T, Lüdemann W, von Rautenfeld DB, Samii M. Dynamic properties of lymphatic pathways for the absorption of cerebrospinal fluid. *Acta Neuropathol*. 1997;94:493–498.
64. Johnston M, Zakharov A, Papaiconomou C, Salmasi G, Armstrong D. Evidence of connections between cerebrospinal fluid and nasal lymphatic vessels in humans, non-human primates and other mammalian species. *Cerebrospinal Fluid Res*. 2004;1:2.
65. Eklund A, Jóhannesson G, Johansson E, et al. The pressure difference between eye and brain changes with posture. *Ann Neurol*. 2016;80:269–276.
66. Fremont-Smith F, Kubie LS. The relation of vascular hydrostatic pressure and osmotic pressure to the cerebrospinal fluid pressure. *Res Publ Assoc Res Nerv Ment Dis*. 1929;8: 104–129.

Investigative Ophthalmology & Visual Science